

## Article

# Catalytic Characterization of Synthetic K<sup>+</sup> and Na<sup>+</sup> Sodalite Phases by Low Temperature Alkali Fusion of Kaolinite during the Transesterification of Spent Cooking Oil: Kinetic and Thermodynamic Properties

Mohamed Adel Sayed<sup>1,2</sup>, Jamaan S. Ajarem<sup>3</sup>, Ahmed A. Allam<sup>4</sup>, Mostafa R. Abukhadra<sup>1,5,\*</sup> , Jianmin Luo<sup>6</sup>, Chuanyi Wang<sup>7</sup> and Stefano Bellucci<sup>8</sup> 

<sup>1</sup> Materials Technologies and Their Applications Lab, Geology Department, Faculty of Science, Beni-Suef University, Beni-Suef 62514, Egypt

<sup>2</sup> Department of Chemistry, Faculty of Science, Beni-Suef University, Beni-Suef 62514, Egypt

<sup>3</sup> Zoology Department, College of Science, King Saud University, Riyadh 11362, Saudi Arabia

<sup>4</sup> Zoology Department, Faculty of Science, Beni-Suef University, Beni-Suef 62514, Egypt

<sup>5</sup> Geology Department, Faculty of Science, Beni-Suef University, Beni-Suef 65211, Egypt

<sup>6</sup> School of Chemistry and Civil Engineering, Shaoguan University, Shaoguan 512005, China

<sup>7</sup> School of Environmental Science and Engineering, Shaanxi University of Science and Technology, Xi'an 710021, China

<sup>8</sup> INFN-Laboratori Nazionali di Frascati, Via E. Fermi 54, 00044 Frascati, Italy

\* Correspondence: abukhadra89@science.bu.edu.eg



**Citation:** Sayed, M.A.; Ajarem, J.S.; Allam, A.A.; Abukhadra, M.R.; Luo, J.; Wang, C.; Bellucci, S. Catalytic Characterization of Synthetic K<sup>+</sup> and Na<sup>+</sup> Sodalite Phases by Low Temperature Alkali Fusion of Kaolinite during the Transesterification of Spent Cooking Oil: Kinetic and Thermodynamic Properties. *Catalysts* **2023**, *13*, 462. <https://doi.org/10.3390/catal13030462>

Academic Editors: De Fang and Yun Zheng

Received: 21 January 2023

Revised: 17 February 2023

Accepted: 20 February 2023

Published: 22 February 2023



**Copyright:** © 2023 by the authors. Licensee MDPI, Basel, Switzerland. This article is an open access article distributed under the terms and conditions of the Creative Commons Attribution (CC BY) license (<https://creativecommons.org/licenses/by/4.0/>).

**Abstract:** The mineral raw Egyptian kaolinite was used as a precursor in the synthesis of two sodalite phases (sodium sodalite (Na.SD) and potassium sodalite (K.SD)) according to the low alkali fusion technique. The synthesized Na.SD phase demonstrates enhanced total basicity (6.3 mmol OH/g), surface area (232.4 m<sup>2</sup>/g), and ion exchange capacity (126.4 meq/100 g) compared to the K.SD phase (217.6 m<sup>2</sup>/g (surface area), 96.8 meq/100 g (ion exchange capacity), 5.4 mmol OH/g (total basicity)). The catalytic performance of the two sodalite phases validates the higher activity of the sodium phase (Na.SD) than the potassium phase (K.SD). The application of Na.SD resulted in biodiesel yields of 97.3% and 96.4% after 90 min and 60 min, respectively, while the maximum yield using K.SD (95.7%) was detected after 75 min. Robust base-catalyzed reactions using Na.SD and K.SD as catalysts were suggested as part of an operated transesterification mechanism. Moreover, these reactions exhibit pseudo-first order kinetics, and the rate constant values were estimated with consideration of the change in temperature. The estimated activation energies of Na.SD (27.9 kJ.mol<sup>-1</sup>) and K.SD (28.27 kJ.mol<sup>-1</sup>) reflected the suitability of these catalysts to be applied effectively under mild conditions. The essential thermodynamic functions, such as Gibb's free energy (65.16 kJ.mol<sup>-1</sup> (Na.SD) and 65.26 kJ.mol<sup>-1</sup> (K.SD)), enthalpy (25.23 kJ.mol<sup>-1</sup> (Na.SD) and 25.55 kJ.mol<sup>-1</sup> (K.SD)), and entropy (−197.7 J.K<sup>-1</sup>.mol<sup>-1</sup> (Na.SD) and −197.8 J.K<sup>-1</sup>.mol<sup>-1</sup> (K.SD)), display the endothermic and spontaneous nature of the two transesterification systems.

**Keywords:** alkali ions; sodalite; transesterification; kinetics; thermodynamic; mechanism

## 1. Introduction

The greenhouse effect, environmental side effects of utilizing fossil fuels, depletion of fossil fuel supplies, and rising crude oil prices exhibit notable negative consequences on the world economy and the safety of our ecosystem. Therefore, developing and introducing additional and sustainable energy sources with eco-friendly and renewable properties are the main concern and interest of researchers, governments, and environmental authorities [1,2]. Generally, biofuels such as biodiesel were assessed in several studies as clean, low-cost, sustainable, effective, and non-toxic alternative fuels [3]. As a fuel, the

commonly developed biodiesel products exhibit notable high lubricant properties, viscosity, and an acceptable flash point ( $>130$  °C) [4]. Moreover, as biodiesel products are sulfur and aromatic-free fuels, they burn cleaner than commercial diesel, giving them significant environmental value [5,6].

Recently, numerous studies have been introduced to utilize fatty acid methyl esters (FAMEs) to produce manufactured products such as lubricants [7], stabilizing agents for polyvinyl chloride [8], plasticizer [9], surfactants, corrosion inhibitors, and water repellents [10,11]; additionally, it can be used for the production of gas, fatty alcohol, and hydrocarbon, which form the standard raw materials for chemical industries [11]. Chemically, biodiesel is known as a series of fatty acid methyl esters (FAME) that can be obtained by the facile transesterification processes of edible or non-edible vegetable oils as well as animal fats as sources of triglyceride with short-chain alcohols (methyl alcohol or ethyl alcohol) in the presence of appropriate heterogeneous or homogenous catalysts [12,13]. However, several triglyceride feedstocks were evaluated during the production of biodiesel (spent oil [14], palm oil [15], virgin cottonseed oil [16], and rubber seed oil [17]). Their availability, accessibility, cost, and suitability to various climatic conditions are essential factors to consider during the selection of the feedstock [18]. Therefore, several studies were introduced in later periods to assess the possible extraction of biodiesel from spent or waste cooking oil, which can act as low-cost, commercial, and recyclable precursors [19].

Most of the previous studies demonstrated a controlling effect of the incorporated catalyst on the efficiencies and rate of the transesterification reactions, in addition to the physical properties of the obtained biodiesel [20].  $H_2SO_4$ , NaOH, and KOH are common and effective catalysts for homogeneously catalyzed transesterification reactions, and have resulted in significant biodiesel yields after acceptable periods and at moderate temperature values [21,22]. However, homogeneous transesterification is an effective process; it is associated with huge quantities of toxic effluent as a byproduct, complex separation processes, and a low recyclability value, which pose several environmental restrictions on its commercial applications [23]. The reported technical and environmental advantages of heterogeneous catalysts, which are known as multi-phase catalysts, over homogeneous catalysts strongly make them an essential part in the generation of biodiesel [24]. These advantages involve their high reusability, the facile separation process involved, their low energy consumption, and the fact that it creates no toxic effluents as by-products [25,26]. Therefore, great efforts have been made to introduce new species of effective heterogeneous catalysts or to enhance the catalytic performances of the commonly used catalysts [3].

Natural and synthetic structures of alkali-enriched ( $K^+$ ,  $Na^+$ , and  $Ca^{2+}$ ) aluminosilicate, especially the zeolite phases, are in a highly recommended class of multi-phase catalysts in the potential transesterification of various types of vegetable oils as well as their spent products [13,27]. This is due to their affordable costs, simple production processes, the availability of their precursors, and their significant physicochemical properties [12,28,29]. The synthetic phases of zeolite display a notable and significant micro-porous structure, surface area, ion exchangeability, thermal stability, surface reactivity, chemical and crystalline flexibility, dispersion properties, and mechanical stability [30–32]. Generally, zeolite is a crystalline, microporous, and hydrated aluminosilicate material that is enriched in alkaline earth and/or alkaline ions. Structurally, it consists of  $SiO_4$  and  $Al_2O_4$  tetrahedral units and their connection by three-dimensional corner oxygen sharing, forming a series of linked cages with highly ordered structural nanochannels or pores [33,34]. Several types of synthetic zeolite (sodalite, zeolite-A, cancrinite, zeolite-P, zeolite-Y, and zeolite-X) were studied as catalysts; they are still part of an active and attractive research area considering the insufficient studies that were introduced to describe the kinetics and mass transfer properties of their transesterification catalytic systems [35]. Moreover, several studies demonstrated notable changes in their morphology as well as their main physicochemical properties, including their porosity, crystalline degree, surface area, ion exchange capacity, basicity, and adsorption affinity in terms of the type of the incorporated raw materials and synthesis conditions (temperature, time interval, degree of alkalinity, and the type of

alkaline solution) [27,30,36]. Recently, the production of synthetic zeolite phases by alkali fusion methods followed by a hydrothermal treatment was recommended strongly for the synthesis phases of zeolite with enhanced stability, crystallinity, basicity, and ion exchange capacity [37,38].

Based on the previous consideration, the presented study here focuses on the kinetic and thermodynamic properties of synthetic zeolite-based catalysts in the transesterification of waste cooking oil. The assessed zeolite phases are two sodalite forms (sodium sodalite (Na.SD) and potassium sodalite (K.SD)), which were produced from natural Egyptian kaolinite by the alkali fusion method. The catalytic performances of the two sodalite phases were determined experimentally and theoretically based on detailed kinetic and thermodynamic studies considering the types of dominant alkaline ions.

## 2. Results and Discussion

### 2.1. Characterization of the Catalysts

The following formation of the zeolite phases, the XRD patterns of the raw kaolinite, as well as the synthetic samples, were presented in Figure 1. The starting precursor exhibited the typical pattern of highly crystalline kaolinite with its notable peaks at about  $12.3^\circ$  (001),  $24.9^\circ$  (002), and  $26.6^\circ$  (111) (XRD. No. 04-012-5104). The zeolite samples, prepared either by using NaOH or by KOH, showed the typical patterns of sodalite (Ref. Code. 04-009-5259) (Figure 1A). The identification peaks of sodalite, which was prepared using NaOH (Na.SD), were marked at  $14.33^\circ$  (110),  $24.69^\circ$  (221),  $31.84^\circ$  (310),  $35^\circ$  (222),  $38.2^\circ$  (321), and  $43.09^\circ$  (330) (Figure 1A). Those of the synthetic sodalite prepared using KOH (K.SD) were marked at  $14.48^\circ$  (110),  $24.76^\circ$  (221),  $31.98^\circ$  (310),  $35.09^\circ$  (222),  $38.44^\circ$  (321), and  $43.22^\circ$  (330) (Figure 1A). The slight deviation in the observed positions of the diffraction peaks of K.SD, compared to those of Na.SD, reflects the effect of the alkaline ions on the structure of sodalite considering the ionic radius of these ions ( $1.94 \text{ \AA}$  ( $\text{Na}^+$ ) and  $1.34 \text{ \AA}$  ( $\text{K}^+$ )) and the substitution capacity within the zeolite structure. This effect was also made evident by the average crystallite's size calculated according to the Scherrer equation ( $D = 0.9\lambda/W \cos\theta$ ), where  $W$  is the full width at half maximum in radians,  $\theta$  is the Bragg's angle, and  $\lambda$  is the X-ray wavelength ( $\text{CuK}\alpha = 0.15405 \text{ nm}$ ). The synthetic K.SD phase exhibited a smaller crystallite size (34.2 nm) than the synthetic Na.SD phase did (40.3 nm).

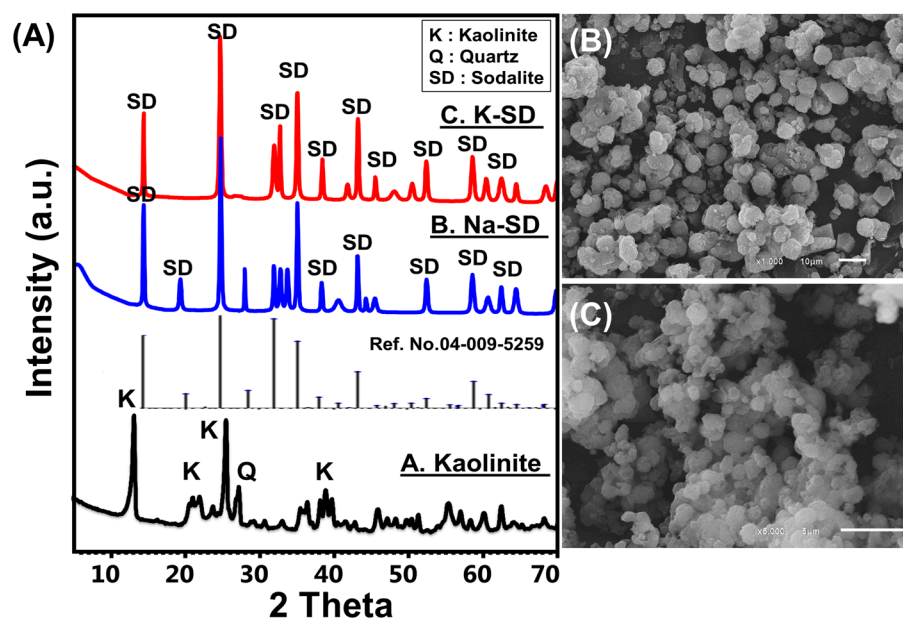


**Figure 1.** XRD patterns of kaolinite and the synthetic sodalite phases (A), SEM image of Na-sodalite (Na.SD) (B), and SEM image of K-sodalite (K.SD) (C).

The formation of the sodalite was confirmed also by the morphological transformation of the raw kaolinite material from characteristic pseudo-hexagonal flakes into different forms (Figure 1B,C). The two obtained sodalite phases exhibited notable changes in morphology. While the Na.SD particles showed well-developed spherical grains commonly separated from each other, the K.SD particles appeared as aggregates of agglomerated grains with spherical to cubic shapes (Figure 1C).

Moreover, the determined FT-IR spectra reflect the significant change from the kaolinite structure into the zeolitic tectosilicate structure of sodalite (Figure 2). The spectrum of kaolinite demonstrates the existence of structural Si-OH ( $3689\text{ cm}^{-1}$ ), structural Al-OH ( $3622$  and  $912\text{ cm}^{-1}$ ), adsorbed O-H ( $1641\text{ cm}^{-1}$ ), Si-O ( $787$  and  $456\text{ cm}^{-1}$ ), Si-O-Al ( $526$  and  $680\text{ cm}^{-1}$ ), and Si-O-Si ( $1020\text{ cm}^{-1}$ ) as the characteristic chemical groups of natural kaolinite minerals (Figure 2A) [38]. The estimated spectra of Na.SD and K.SD reveal that there was considerable shifting in the corresponding bands of the essential aluminosilicate chemical groups. This strongly signifies the impact of the alkaline alteration processes, which is associated with significant leaching effects on the structural Si and Al ions in addition to the remarkable exposure of the active siloxane groups [39]. Moreover, the detected bands within the range from  $630$  to  $635\text{ cm}^{-1}$  denote the known symmetric stretching of the Si-O-Si group of the structural units of zeolite (Figure 2B,C) [40]. The formation of zeolite was also confirmed by the identified band around  $1475\text{ cm}^{-1}$ , which signifies the presence of trapped zeolitic water within the internal channels of the zeolite structure [41].

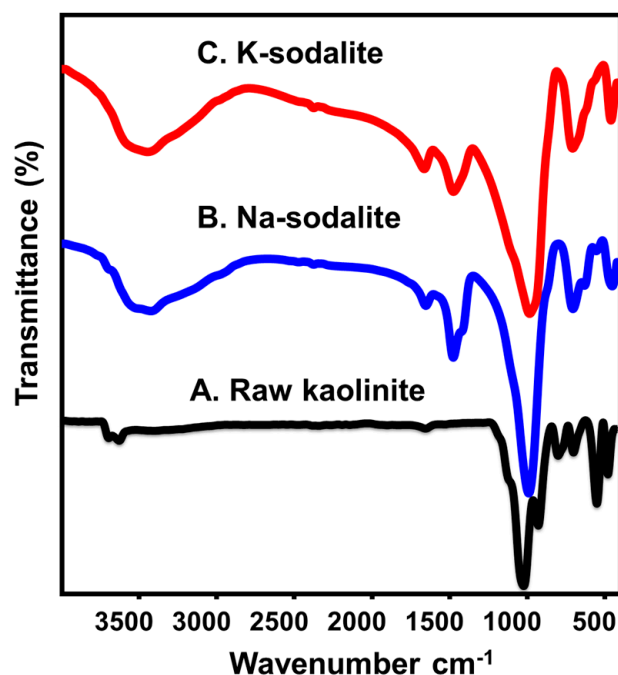


**Figure 2.** The FT-IR spectra of kaolinite (A), synthetic Na.SD (B), and synthetic K.SD (C).

The reported changes in the morphology as well as in the chemical and crystalline structure significantly affected the textural and physicochemical properties of the synthetic sodalite phases (Table 1). The synthetic Na.SD phase exhibited a higher surface area ( $232.4\text{ m}^2/\text{g}$ ), ion exchange capacity ( $126.4\text{ meq}/100\text{ g}$ ), and total basicity ( $6.3\text{ mmol OH}/\text{g}$ ) than the determined values of K.SD ( $217.6\text{ m}^2/\text{g}$  (surface area),  $96.8\text{ meq}/100\text{ g}$  (ion exchange capacity),  $5.4\text{ mmol OH}/\text{g}$  (total basicity)) (Table 1). While the high surface area and total basicity of the Na.SD compared to those of the K.SD induced the former's catalytic activity, its high ion exchange capacity might have been caused by adverse and saponification effects during the transesterification reactions.

**Table 1.** The textural properties of kaolinite, K.SD, and Na.SD.

Sample	Surface Area	Total Pore Volume	Average Pore Size	Cation Exchange Capacity	Total Basicity
Kaolinite	10 m <sup>2</sup> /g	0.072 cm <sup>3</sup> /g	43.2 nm	—	—
K.SD	217.6 m <sup>2</sup> /g	0.214 cm <sup>3</sup> /g	9.7 nm	96.8 meq/100 g	6.3 mmol OH/g
Na.SD	232.4 m <sup>2</sup> /g	0.247 cm <sup>3</sup> /g	7.4 nm	126.4 meq/100 g	5.4 mmol OH/g

## 2.2. Transesterification Results

### 2.2.1. Effect of the Experimental Variables

#### Effect of Transesterification Intervals at Different Temperatures

The experimental impact of the transesterification duration on the formation rate and percentages of methyl ester was studied regularly from 15 min up to 120 min. This was evaluated with consideration of the different values for the transesterification temperature (40 °C up to 80 °C) and the fixed values for the other affecting parameters (methanol-to-oil molar ratio: 12:1 and the catalyst load: 2.5 wt.%) (Figure 3A,B). A satisfactory transesterification duration is essential to ensure the effective interaction and miscibility between the different reactants, and doing so turn achieved the best conversion rate and efficiency [42]. Therefore, the short intervals observed in the K.SD and Na.SD transesterification systems were associated with poor homogeneity, low miscibility, and high mass resistance in the conversion systems [13,43]. This resulted in the notably low conversion rates of TG into FAME during the initial intervals of the reactions at all the investigated temperature values, either in the presence of Na.SD or K.SD (Figure 3A,B). Consequently, expanding the reaction duration at a significant rate prompts the miscibility properties in the system, which enhances the formation percentages of FAME. This can be observed up to certain intervals at which the used Na.SD (90 min) and K.SD (75 min) achieved their best catalytic activities in terms of the determined yields (Figure 3A,B). Beyond the previously mentioned intervals, the Na.SD- and K.SD-based transesterification systems showed a considerable decrease in the quantities of the produced FAME regardless of the temperature. This adverse effect was attributed to the reversible nature of the methanolysis processes in addition to the expected acceleration of some of the side reactions, which include the re-dissolving of the existing glycerol into alcohol [12,42].

The experimental influence of the transesterification temperature on the activity of the K.SD and Na.SD catalysts was assessed experimentally from 40 °C to 80 °C based on the measured yields of FAME (Figure 3A,B). The measured FAME and the total yields accelerated strongly with the increase in the transesterification temperature up to 70 °C, using both Na.SD (94.8% yield) and K.SD (88.6% yield), which is close to the reported boiling point of the methyl alcohol (Figure 3A,B). This demonstrates that the transesterification processes were endothermic reactions and that their threshold kinetic energies enhanced the mass transfer properties within the system between the different reactants [44–46]. The significant loss in the methanol content as a result of its evaporation from the system during the conduction of the tests up to 70 °C had significant adverse impacts on the efficiency of the production of FAME [47].

The determined yields of FAME as well as the recognized catalytic properties of Na.SD and K.SD as functions of the assessed factors (temperature and reaction duration) validate the significant differences between the two sodalite phases in their catalytic activities. The sodium-rich phase (Na.SD) exhibited higher catalytic properties than the potassium-rich phase (K.SD) did at lower intervals. This was credited to the determined high basicity and surface area of the Na.SD compared to the K.SD, which reflect the significant effect of the species of the used alkaline solutions on the synthesis of the sodalite catalyst.

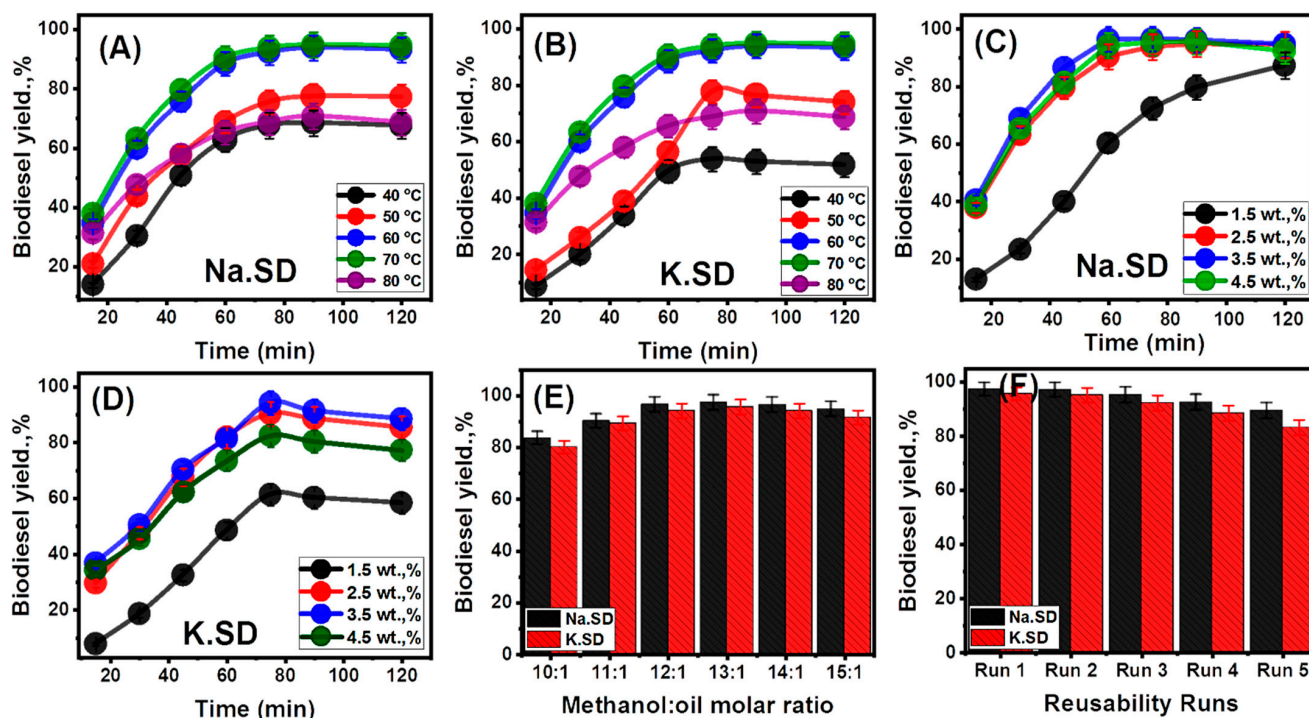


**Figure 3.** The effect of (A) the transesterification duration in different temperature conditions on the catalytic activity of Na.SD, (B) the transesterification duration on the catalytic activity of K.SD, (C) the effect of the catalyst loading of Na.SD on the obtained biodiesel yield, (D) the effect of the catalyst loading of K.SD on the obtained biodiesel yield, (E) the methanol-to-oil molar ratio, and (F) the recyclability properties of Na.SD and K.SD as heterogeneous catalysts.

#### Effects of the Catalysts Dosages on FAME Yield

The impact of the Na.SD and K.SD dosages on the efficiency of the production of FAME was studied from 1.5 wt.% up to 4.5 wt.%. This was evaluated with consideration of the different values of the transesterification duration (15 min up to 120 min) and of the fixed values of the other affecting parameters (methanol-to-oil molar ratio: 12:1 and temperature: 70 °C). Considering the best identified transesterification durations in the presence of Na.SD (90 min) and K.SD (75 min), the incorporated dosages of them exhibited a notable enhancement of the produced FAME as well as of the rate of the production of FAME (Figure 3C,D). This was detected within the assessed range from 1.5 wt.% (79.7% yield (Na.SD) and 60.2% yield (K.SD)) to 3.5 wt.% (96.8% yield (Na.SD) and 91.4% yield (K.SD)) (Figure 3C,D). The incorporation of Na.SD and K.SD at satisfactorily high dosages were associated with a significant enhancement of the availability of the effective catalytic sites as well as of the interactive interfaces between the catalyst grains and the liquid phases [44]. This resulted in the reported enhancement of the generation quantities of FAME as well as of the actual transformation rates of triglycerides. However, the conducted tests in the presence of a dosage of 4.5 wt.% of both Na.SD and K.SD demonstrated observable adverse effects on the quantities of formed FAME (Figure 3C,D). This was reported in the literature as a result of the negative impacts of the presence of dosages beyond the threshold in the system on the viscosity, homogeneity, and mass transfer resistance between the spent oil, methanol, the sodalite particles as reactants [20,48,49].

#### Effect of Methanol-to Oil Molar Ratio

The molar ratio of methyl alcohol to triglyceride content is a crucial parameter that controls the efficiency of the generation of biodiesel during the conversion of the incorporated spent cooking oil [1,50]. According to stoichiometry, the best transesterification efficiency can be achieved by the successful reaction between 3 moles of methyl alcohol

and 1 mole of triglyceride, which normally results in 3 moles of FAME in addition to 1 mole of glycerol [47]. According to Lee Chatelier's concept, the alcohol content in the systems should be preserved at levels higher than the reported stoichiometric value to keep the reaction progressing in the forward direction and to avoid the reversible properties of such transesterification processes [1,44]. The actual impact of the molar ratio of the alcohol to the oil on the Na.SD and K.SD transesterification systems were studied from 10:1 to 15:1 (Figure 3E). This was evaluated with consideration of the best values of the other affecting parameters obtained from the previously mentioned tests (sodalite dosage: 3.5 wt.%; temperature: 70 °C; and duration time: 90 min (Na.SD) and 75 min (K.SD)).

The efficiency of the production of FAME as well as the rate of its production were enhanced notably in terms of the increase in the adjusted molar ratio of the used alcohol up to 13:1 either in the presence of Na.SD (97.3%) or K.SD (95.7%) (Figure 3E). An excess in methanol within the recommended stoichiometric levels significantly enhances the miscibility properties of the system by reducing the viscosity as well as the mass transfer resistance [50]. Furthermore, high methanol ratios exhibit remarkable acceleration effects on the collision or the interaction processes between the triglycerides as dissolved molecules and the surface of the sodalite solid particles [44]. However, this was detected up to a certain ratio (14:1) in the experiment, and then the excess in the used alcohol caused observable adverse properties that resulted in low FAME yields, especially at the highest level of the adjusted methanol/oil ratio (15:1) (94.8% (Na.SD) and 91.6% (K.SD)) (Figure 3E). This reversible effect was documented in previous studies and was illustrated as being a result of the predicted re-dissolving of the glycerol molecules within the excess methanol beyond the stoichiometric levels. This negatively affected the balance between the biodiesel and glycerol in the transesterification reaction and effective phase separation, causing reversible reactions [13,51]. Moreover, the free alcohol molecules might create deactivation effects on the essential active catalytic chemical groups of the sodalite particles. Also, this might be associated with the significant conversion of them into non-preferred emulsifier centers after the expected inversion of the polar groups [52,53].

#### Recyclability of Na.SD and K.SD Catalysts

The stability and recyclability potentials of the prepared Na.SD and K.SD phases as solid heterogeneous catalysts were studied as critical parameters during the assessment of the products for realistic and commercial applications. The extracted Na.SD and K.SD particles after the transesterification processes were washed firstly with methanol as a common solvent of adsorbed organic molecules (fatty acid and glycerol) on their surfaces. This step was repeated for five runs, each run taking about 10 min, and then the particles were washed with distilled water for 15 min. After the washing step, the obtained Na.SD and K.SD were dried at 80 °C for about 12 h and then re-used again in a new transesterification test. All the recyclability tests were adjusted to the experimentally detected best values (sodalite dosage: 3.5 wt.%; temperature: 70 °C; methanol/oil ratio: 13:1; and duration time: 90 min (Na.SD) and 75 min (K.SD)) (Figure 3F).

Based on the measured results, Na.SD showed considerable recyclability properties and stability as an incorporated basic catalyst in the heterogeneous catalytic transesterification systems compared to K.SD considering the number of runs (5 runs) in which it was reused. In terms of the reusability of Na.SD, it reflected its ability to obtain FAME yields beyond 97% after two runs, beyond 95% after three runs, and above 89% after five runs (Figure 3F); additionally, the reusability properties of K.SD allowed it to obtain FAME yields higher than 95% and 92% after two and three runs, respectively, yet it is accompanied by a noticeable decrease at the fifth run, with a FAME yield of 83% (Figure 3F). The observable dwindling in the FAME yield and the activities of both the Na.SD and K.SD with the regular repetition of the reusing runs might be credited to the expected leaching of some of the exchangeable Na<sup>+</sup> and K<sup>+</sup> ions within the structure of sodalite during the washing and transesterification processes [32,54]. Furthermore, the over-accumulation of glycerol on the

surfaces of their particles might have negatively affected the exposure of the active sites and might have deactivated them as active centers [12].

### 2.2.2. Physical and Chemical Properties of The Obtained Biodiesel

Both the ASTM D-6751 and EN 14214 biodiesel international standards were used to assess the physical qualifications of the biodiesel products obtained by the Na.SD and K.SD transesterification systems to be used as safe and suitable biofuel (Table 2). According to the presented criteria, the products by obtained both the Na.SD and K.SD exhibited acceptable viscosity and density for their use directly as suitable fuel. Additionally, the cetane index of the two biodiesel products is more than 45, signifying that their combustion quality and ignition delay time are acceptable for their use as effective and safe fuels in engines [13]. The determined flashpoint values as well as the calorific values of two biodiesel products validate the significant safety of their properties, as commercial products, for their handling and transportation, which is in agreement with the low values of the measured pour and cloud points (Table 2).

**Table 2.** The physical properties of the biodiesel products using Na.SD and K.SD catalysts.

Contents	ASTM D-6751	EN 14214	Na.SD	K.SD
Viscosity (mm <sup>2</sup> /s)	1.9–6	3.5–5	3.72	3.24
Moisture content (wt.%)	<0.05	<0.05	0.041	0.032
Flash point (°C)	>93	>120	134.2	129.8
Calorific value (MJ/kg)	—	>32.9	37.4	36.5
Cloud point (°C)	−3 to 15	—	5.7	5.33
Pour point (pp)	−5 to 10	—	6.2	5.7
Cetane number	≥47	≥51	54.3	52.5
Density (g/cm <sup>3</sup> )	0.82–0.9	0.86–0.9	0.87	0.84
Acid value (Mg/KOH/g)	≤0.5	≤0.5	0.42	0.37

The determined species of the formed esters, according to the GC-MS analysis, demonstrated the existence of oleic acid, palmitoleic acid, and linoleic acid methyl esters as the dominant phases of the generated fatty acid methyl esters (FAME) (Table S1). Moreover, other phases were detected but at small percentages, such as myristic acid, palmitic acid, eicosanoic acid, stearic acid, caprylic acid, and behenic acid methyl esters (Table S1).

### 2.2.3. The Suggested Mechanism

By considering the differential spectra of the fresh Na.SD and K.SD as well as their used products after the performed experiments, their effective transesterification mechanisms can be illustrated. The notable observation of the identified FT-IR bands of the CH<sub>2</sub> aliphatic group as well as of the ester carbonyl group in the spectra of the used products validates the considerable adsorption of triglyceride molecules by the active sites of both Na.SD and K.SD. The non-detection of any bands related to the formation of sodium or potassium methoxides suggested no effects of the interaction between the active sites of the two sodalite phases and the methanol molecules on their mechanistic behaviors during the transesterification processes [12]. Therefore, it is suggested here that the transesterification on the surfaces of the Na.SD and K.SD initiated significant interactions between the basic alkali bonds of the sodalite structures (Na-O and K-O) and the triglycerides of the transformed oil (Figure 4) [44]. This suggestion is supported by the previously identified CH<sub>2</sub> aliphatic and ester carbonyl groups [55,56]. The previous step was followed with surface interaction processes between the triglyceride molecules and the alcohol molecules at the active functional sites on the surfaces of the Na.SD and K.SD (Figure 5). During this interaction, the position of the O in Na-O and K-O was substituted with the methoxide molecules (CH<sub>3</sub>O-), forming fatty acid methyl ester. After that, the effective capturing of the hydrogen ions from the system by the starting glycerol backbone resulted in the formation of stable glycerol molecules that desorbed immediately from the surfaces of the Na.SD and K.SD

(Figure 4) [1]. This caused the evacuation of the effective active catalytic centers and their transformation into free sites for new runs of triglyceride interaction. Considering the previously reported mechanistic steps, the high surface area and total basicity of the Na.SD accelerated the transesterification rate at a higher efficiency compared to K.SD, reflecting the significant impacts of the used types of alkali on the procedures of the synthesis of sodalite from kaolinite as well as on the applied synthesis methodology.

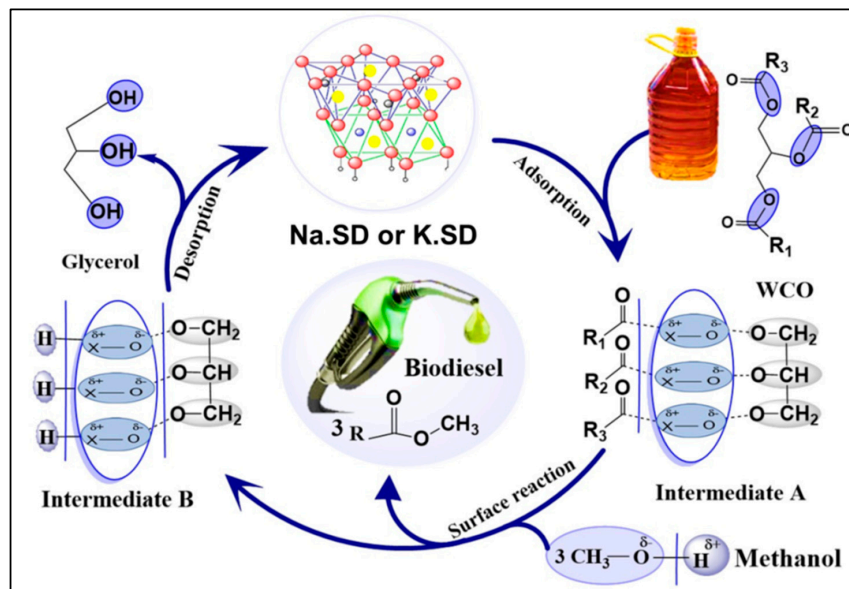


Figure 4. Schematic diagram of the transesterification of waste cooking oil into biodiesel using the synthetic Na.SD and K.SD catalysts.

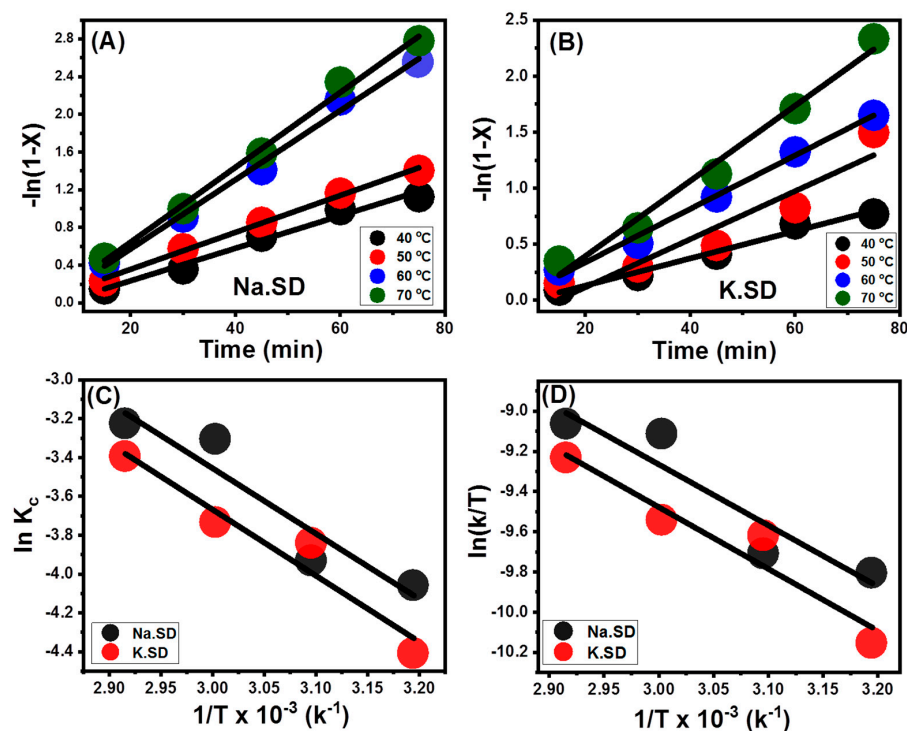


Figure 5. Results of the fitting of the biodiesel yields of Na.SD and K.SD with the pseudo-first-order kinetic model (A,B), with the Arrhenius equation (C), and with the Eyring–Polanyi equation (D).

#### 2.2.4. Kinetics and Thermodynamics

The kinetic and thermodynamic functions of the Na.SD- and K.SD-based transesterification systems as well as their significance were evaluated based on the reported procedures in Section 2. The essential kinetic functions that were investigated in this study were the activation energy and reaction rate constant, while the obtained thermodynamic functions were the activation entropy, activation enthalpy, and Gibb's free energy.

##### Kinetic Studies

##### The Reactions Rate Constants

The rate constant ( $K_c$ ) values of the occurred transesterification reactions based on the Na.SD and K.SD systems were obtained as mathematical parameters for the linear regression relations between  $-\ln(1-X)$  vs. the reaction duration in min (Figure 5A,B). This was assessed with consideration of the experimental range of temperatures from 40 °C to 70 °C and the duration range from 15 min to 75 min after the fixation of the other factors (methanol-to-oil molar ratio: 12:1 and the catalyst load: 2.5 wt.). The fitting processes demonstrated the pseudo-first-order kinetic properties of the reactions that occurred during the conversion of waste cooking oil based on the Na.SD and K.SD transesterification systems with considerably high determination coefficients ( $R^2 > 0.87$ ) (Figure 5A,B). This kinetic behavior validates the occurrence of the reaction according to the three significant steps of adsorption, surface interaction, and desorption progressive processes that are in notable agreement with the obtained findings of the FT-IR analysis of the used Na.SD and K.SD particles [29,42]. The observable increases in the theoretically estimated values of the  $K_c$  according to the temperature of the tests exhibited notable agreement with the observed experimental behaviors, including the positive influence of the temperature on the catalytic systems of the Na.SD and K.SD (Table 3). Moreover, the  $K_c$  values of the reactions that occurred in the presence of Na.SD were higher than those of the accomplished reactions in the presence of K.SD, validating the higher catalytic activity of the sodium sodalite phase.

**Table 3.** The estimated values of the determination coefficient and rate constant of the pseudo-first-order kinetic model.

Catalyst	Temperature (°C)	$K_c$ (min <sup>-1</sup> )	( $R^2$ )
Na.SD	40	0.01723	0.97813
	50	0.01958	0.99603
	60	0.03666	0.99031
	70	0.0397	0.99457
K.SD	40	0.01214	0.97264
	50	0.02143	0.871
	60	0.02386	0.9912
	70	0.03353	0.97781

##### The Reaction Activation Energy and Pre-Exponential Values

The regression relations between the rate constants and the values of  $1/T$  previously estimated according to the Arrhenius equation were used to estimate the values of the activation energy ( $E_a$ ) of the transformation reactions of the spent oil in the Na.SD and K.SD transesterification systems (Figure 5C; Table 4). The calculated activation energies during the transesterification processes in presence of the Na.SD and K.SD catalysts were 27.9 kJ.mol<sup>-1</sup> and K.SD 28.27 kJ.mol<sup>-1</sup>, respectively, while the obtained pre-exponential factors for the occurred reactions by Na.SD and K.SD were 758.94 min<sup>-1</sup> and 688.33 min<sup>-1</sup>, respectively (Table 4). It was reported that the transesterification systems that exhibit low activation energy were characterized by low energy barriers and could achieve signified yields and efficiencies at low to moderate operating temperatures [57]. Regarding the pre-exponential factor, the system which showed high values exhibited enhanced collision properties and enhanced chances of interaction between the different reactants and the

exposed active catalytic centers of sodalite, and this in turn induced the methylation of the triglyceride molecules. This, in addition to the previously mentioned physicochemical properties, illustrates the higher catalytic activity of Na.SD compared to K.SD.

**Table 4.** The activation energy and pre-exponential values of the performed transesterification reactions using Na.SD and K.SD.

Parameters	Na.SD	K.SD
Slope	−3.36	−3.40
Intercept	6.63	6.534
Determination coefficient ( $R^2$ )	0.848	0.907
Activation energy ( $\Delta E^*$ ) ( $\text{kJ}\cdot\text{mol}^{-1}$ )	27.9	28.27
Pre-exponential value (A) ( $\text{min}^{-1}$ )	758.94	688.33

#### The Thermodynamic Functions (Enthalpy, Entropy, and Gibb's Free Energy)

The main thermodynamic functions of the Na.SD- and K.SD-based transesterification reactions were obtained as mathematical theoretical parameters of the fitting results with the Eyring–Polanyi equation with consideration of the linear regression relations between  $\ln(K_c/T)$  and  $1/T$  (Figure 5D, Table 5). Based on the notable positively signed values of enthalpy ( $\Delta H^*$ ) ( $25.233 \text{ kJ}\cdot\text{mol}^{-1}$  (Na.SD) and  $25.55 \text{ kJ}\cdot\text{mol}^{-1}$  (K.SD)) and Gibb's free energy ( $\Delta G^*$ ) ( $61.9\text{--}67.836 \text{ kJ}\cdot\text{mol}^{-1}$  (Na.SD) and  $61.93\text{--}67.87 \text{ kJ}\cdot\text{mol}^{-1}$  (K.SD)) validate the spontaneous and endothermic behaviors of the two transesterification systems (Table 5). Moreover, the negatively signed entropy ( $\Delta S^*$ ) values of both Na.SD ( $-197.7 \text{ J}\cdot\text{K}^{-1}\cdot\text{mol}^{-1}$ ) K.SD ( $-197.8 \text{ J}\cdot\text{K}^{-1}\cdot\text{mol}^{-1}$ ) reflects a considerable reduction in the randomness of the reactions that occurred with the elevation in the transesterification temperature.

**Table 5.** The estimated thermodynamic functions of Na.SD and K.SD transesterification systems.

Thermodynamic Parameters	Na.SD	K.SD
Slope	−3.03508	−3.0734
Intercept	−0.16003	−0.25768
$R^2$	0.81843	0.88793
$\Delta H^*$ ( $\text{kJ}\cdot\text{mol}^{-1}$ )	25.233	25.55
$\Delta S^*$ ( $\text{J}\cdot\text{K}^{-1}\cdot\text{mol}^{-1}$ )	−197.7	−197.8
$(\Delta G^*)$ ( $\text{kJ}\cdot\text{mol}^{-1}$ )	40 °C	61.905
	50 °C	63.882
	60 °C	65.859
	70 °C	67.836
		61.936
		63.914
		65.892
		67.87

#### 2.2.5. Comparison Study

The catalytic activities of both Na.SD and K.SD were compared with other assessed basic heterogeneous catalysts in terms of the determined yields in certain experimental conditions. The assessed synthetic sodium and potassium sodalite phases obtained by the low-temperature alkaline fusion of natural kaolinite exhibited higher activity than several investigated products did, these products including synthetic apatite, nickel oxide-based catalysts, Cs modified silica, CaO, CaO/SiO<sub>2</sub>, and kettle limescale (Table 6). Moreover, these results suggest that the alkaline fusion synthesis of sodalite using NaOH, rather than KOH, should be recommended to obtain a more effective catalyst that can achieve promising yields within reasonable time intervals in the presence of low solid dosages and low alcohol content.

**Table 6.** Comparison between the obtained biodiesel yield using Na.SD and K.SD catalysts and other catalysts in the literature.

Catalyst	Time	Temperature (°C)	Methanol/Oil Ratio	Dosage (wt.%)	Yield (%)	References
CaO/SiO <sub>2</sub>	3 h	65	21:1	11	90.2	[58]
Kettle lime scale	15 min	61.7	3:1.7	8.9	93.4	[59]
Zeolite Na-X	8 h	65	6:1	3	83.5	[60]
CaO	3 h	65	20:1	5	95	[61]
Cesium modified silica	3 h	65	20:1	3	90	[62]
Ni/Fe carbonate-fluorapatite	2 h	70	8:1	10	97.5	[63]
Coconut coir husk	3 h	130	12:1	10	89.8	[64]
Diatomite/CaO/MgO	2 h	90	15:1	6	96.4	[50]
Ni/NiO@Diatomite	117 min	63.7	11.6:1	4	93.2	[20]
Na.SD	90 min	70	13:1	2.5	97.3	This study
K.SD	75 min	70	13:1	2.5	95.7	This study

### 3. Experimental Work

#### 3.1. Materials

The kaolinite powder that was used as a precursor was delivered from the Central Metallurgical Research & Development Institute in Egypt after gentle beneficiation steps. NaOH scales (97%; Alfa Aesar, Egypt) as well as KOH pellets (90%; Sigma-Aldrich, Egypt) were used as the sources of the main alkaline ions during the alkali fusion of kaolinite. The spent cooking oil sample tested during the operated transesterification experiments represented a mixture of different commercial samples, which were obtained from different local restaurants. The composition of the incorporated spent cooking oil sample is detailed in Table S2.

#### 3.2. Synthesis of Sodalite Catalysts

The two sodalite phases of sodium sodalite and potassium sodalite were obtained by the alkali fusion of the kaolinite, followed by a gentle hydrothermal alteration step. The kaolinite precursor was mixed in separate experiments with NaOH and KOH with consideration of the weight ratio at 1(kaolinite): 2(alkali hydroxide), and then the resulting mixtures were fused gently at 200 °C for 4 h. The fused products were ground carefully, and about 6 g of each fused product (NaOH/kaolinite and KOH/kaolinite) was homogenized within 100 mL of distilled water at an adjusted temperature of 70 °C while stirring for 2 h. This step was followed by the hydrothermal alteration of the mixtures at 90 °C for 4 h after transferring them into two Teflon-lined stainless steel reactors. By the end of the alteration interval, the reactors were cooled down and the synthesized sodalities fractions were separated from the residual alkaline solutions. Finally, the products were neutralized and washed from the excess alkali ions, dried (85 °C overnight), and labeled as Na.SD (sodium sodalite) and K.SD (potassium sodalite) (Figure 6).

#### 3.3. Characterization Techniques

A transformation of the kaolinite into sodalite zeolite phases occurred, as revealed by the X-ray diffraction patterns determined using an X-ray diffractometer (PANalytical (Empyrean)) within the 5° to 70° determination range. The predicted changes in the chemical groups followed, as revealed by their FT-IR spectra, which were measured by a Fourier Transform Infrared spectrometer (Shimadzu FTIR–8400S) with a frequency range from 400 up to 4000 cm<sup>-1</sup>. A scanning electron microscope (Gemini, Zeiss-Ultra 55) was used to determine and describe the morphological features of the raw and synthesized products based on the SEN images obtained at an accelerating voltage of 30 kV. The

basicity properties were illustrated based on the determined values of the K.SD and Na.SD according to the reported methods by [33]. The ion exchange capacities of both the Na.SD and K.SD, as essential parameters in the transesterification processes, were measured by the  $\text{BaCl}_2$  technique according to the reported procedures by [34]. The textural studies were assessed according to the BET surface area and porosity of the two sodalite phases, which were revealed by the adsorption/desorption isotherm curves obtained using the Beckman Coulter surface area analyzer (SA3100 type).

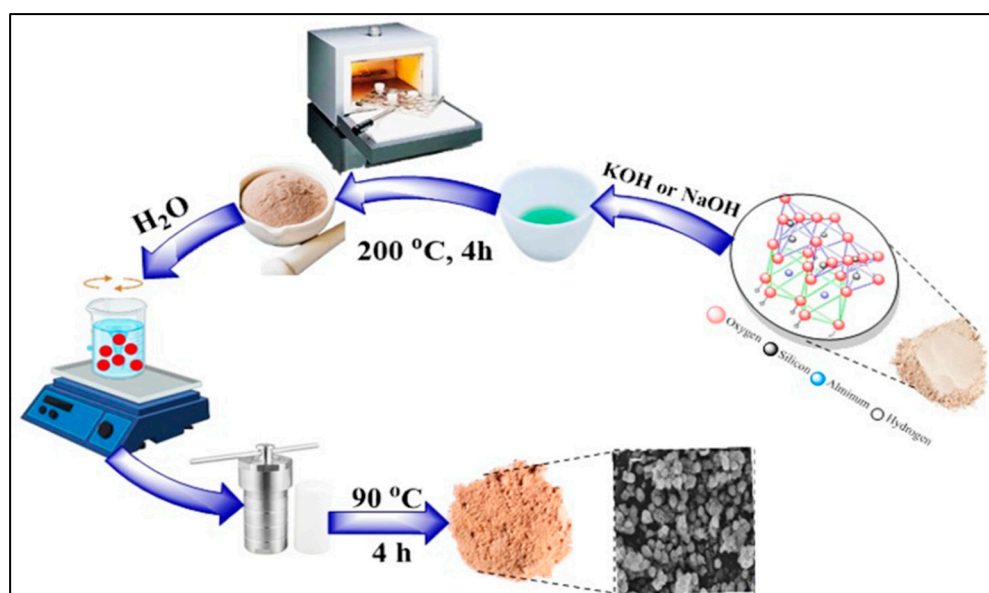


**Figure 6.** Schematic diagram of the synthesis procedures of Na.sodalite and K.sodalite.

### 3.4. Transesterification System

Stoichiometrically, each mol of triglyceride can be transesterified with three mol of methanol, producing one mol of pure glycerol and three mol of fatty acid methyl ester (FAME) (biodiesel). According to the previous stoichiometric base, the transesterification of the investigated spent oil sample was accomplished within a considerable experimental range for the incorporated reactants and operating conditions to attend to the appropriate ratios. All the performed reactions between the incorporated reactants were carried out in a specific reactor, the Teflon autoclave (150 mL), which was attached with a digital magnetic stirrer and hot plate to control the homogenization degree and the temperature according to the selected values. The main variables that were investigated during the study were the methanol molar ratio, sodalite loading, transesterification duration, and temperature, and the best obtained value of each test was considered during the operation of the next test.

The experimental procedures that were followed during the tests involved, firstly, the careful and effective filtration of the collected spent oil samples to get rid of the tough suspensions. Then, a certain volume of the filtrated oil sample was heated directly at  $100\text{ }^{\circ}\text{C}$  for 20 min to get rid of the present water molecules and to avoid the side effects of humidity. After cooling the heated oil sample, the sodalite catalysts (Na.SD and K.SD) were mixed separately with the oil at a certain dosage for 50 min followed by a gradual increase in the operating temperature up to a certain value according to the experimental design. This step is associated with the controlled incorporation of the methanol at an adjustable volume according to the pre-calculated molar ratio to the oil sample for a certain transesterification interval. By completing the reaction duration, the Na.SD and K.SD particles were separated by centrifugation from the liquid phases (biodiesel + glycerol) and were then separated from each other by a glass separating funnel. Then, the obtained sample was left for an additional 24 h to confirm the complete separation of the glycerol content, and this was followed by heating the sample for 3 h at about  $70\text{ }^{\circ}\text{C}$  to certify the effective evaporation

of the rest of the methanol molecules. After that, the quantities as well as the types of the formed FAMEs were determined by gas chromatography coupled with a mass spectroscopy unit (GC-Mass) instrument (Agilent 7890A). The determined values were applied in the direct calculation of the experimentally obtained biodiesel yield (Equation (1)).

$$\text{Biodiesel yield (\%)} = \frac{(\text{weight of biodiesel}) \times \% \text{ FAME}}{\text{weight of triglycerides}} \times 100 \quad (1)$$

### 3.5. Analysis of the FAME Samples

The types, as well as the quantities of the formed fatty acid methyl esters during the transesterification reactions using both N.SD and K.SD, were measured by gas chromatography coupled with a mass spectroscopy unit (GC-Mass) instrument, Agilent-7890A. All the measurements were conducted with the existence of n-hexane as a non-polar solvent of the FAME molecules and methyl heptadecanoate (1  $\mu$ L) as an analytical internal standard. The Agilent-7890A series gas chromatography system used was coupled with a flame ionization detector, split/splitless injector, and capillary column (DB WAX (30 m  $\times$  0.25 m  $\times$  0.25  $\mu$ m)) saturated with a hydrogen carrier and with a 100:1 split proportion. During its operation, the working temperature of the detector as well as the injector was maintained at about 280  $^{\circ}$ C, while the temperature of the oven was adjusted firstly to 120  $^{\circ}$ C and then raised up to 260  $^{\circ}$ C at an accelerating rate of 10  $^{\circ}$ C/min.

### 3.6. Kinetics Studies

The kinetic properties of the Na.SD and K.SD transesterification-based systems were observed within various intervals from 15 min up to 120 min and within an experimental temperature range from 40  $^{\circ}$ C until 70  $^{\circ}$ C with consideration of the other experimental conditions at certain values (catalyst dosage = 2.5 wt.% and methyl alcohol/spent oil molar ratio = 12:1). The transesterification process involves three essential consecutive reversible reactions and all of them include reactions between triacylglycerol- (TG) and methyl-producing diacylglycerols (DG\*) (Equation (2)), monoacylglycerols (MG\*) (Equation (3)), and fatty acid methyl esters (FAME) in addition to glycerol (GL) (Equation (4)) [65]. These reactions reflect the neglected impacts of the transesterification intermediates on the efficiency of the process as the FAMEs molecules can be produced directly during the reaction between the triglycerides and methyl alcohol. Therefore, the overall transesterification of triglycerides can be represented by one step according to Equation (5) [66]. Stoichiometrically, each mol of TG, DG\*, and MG\* react with one mol of alcohol (R-OH) to produce only one mol of GL and 3 mol of FAME [67].



This assumption was suggested based on four essential parameters as follows: (A) the incorporated main reactants of triglycerides, methanol, and solid catalyst particles is distributed homogeneously within the system, (B) the possible occurrence of reverse reactions as well as the changes in the catalyst dosage can be neglected by adjusting the catalyst dosage at an appropriate amount, (C) the incorporated concentration of the methyl alcohol is assumed to be almost constant throughout the transesterification reaction, and (D) the generated intermediates during transesterification reactions are ignored. According to the reported mechanistic steps in the literature, the formation of the FAME by the heterogeneous solid catalyst involves (1) the adsorption of triacylglycerol by the active sites of sodalite as the initial step, (2) a surface reaction between the adsorbed molecules and active catalytic sites, and finally, (3) the desorption of glycerol [43].

### 3.6.1. Adsorption of Triglyceride by Active Sites of Sodalite

The transesterification efficiency of the adsorbed triacylglycerol molecules on the surfaces of both the Na.SD and K.SD as incorporated heterogeneous catalysts and the resulting fatty acid methyl esters are affected by the methanol content rather than by the concentrations of the triglycerides. This process depends essentially on the adsorption of significant quantities of TG molecules on the surfaces of both Na.SD and K.SD according to Equation (6), using the values of the free active catalytic sites (S) and the adsorbed quantities of TG (TG.S). Furthermore, the transesterification rate law can be expressed by Equation (7).



$$r_{ad} = K_a[TG][S] - (K_{-a}[TG.S]) \quad (7)$$

### 3.6.2. Surface Reaction

This step involved significant reactions between the adsorbed TG and the alcohol molecules, where the TG molecules were affected by the nucleophilic attack of a methoxy group (CH<sub>3</sub>O<sup>-</sup>) forming a series of different species of fatty acid methyl esters in addition to the glycerol byproducts. The high affinity of the remaining free sites to the produced GL molecules causes the facile and significant diffusion of the AME molecules according to Equation (8), which uses the quantities of the GL molecules (GL.S) adsorbed by sodalite, and the rate of this surface reaction can be represented by Equation (9) [44].



$$r_s = K_s[R - OH][TG.S] - (K_{-s}[GL.S][FAME]) \quad (9)$$

### 3.6.3. Desorption of Glycerol

The release behavior of the adsorbed GL molecule (GL.S) can be determined according to Equation (10), and the rate law of this reaction can be represented by Equation (11). Based on this equation (Equation (10)) and the other representative equations of the mechanistic steps of transesterification (adsorption and surface reaction), the three steps can be represented by a general equation (Equation (12)) using the total quantities of the free active sites (S<sub>total</sub>). Based on Equation (12), the rate of the surface reaction was modified, as in Equation (13), according to the values of the S<sub>total</sub> instead of those of the TG.S and GL.S.



$$r_d = K_d[GL.S][S] - (K_{-d}[GL][S]) \quad (11)$$

$$[TG.S] \cdot [S_{total}] = [S] + [TG.S] + [GL.S] \quad (12)$$

$$r_s = K_a \cdot K_s [S_{total}] ([TG][R - OH] - [GL][R - COOCH_3]/K_c) / (1 + K_A [TG] + [GL]/K_d) \quad (13)$$

The final representative equation of the general transesterification reaction rate is represented by Equation (14), which uses the rate constant (K<sub>c</sub>) of the reaction, which was estimated according to Equation (15). The general reaction rate equation (Equation (14)) was presented with consideration of four essential factors, these being (1) the fact that the desorption of GL occurred at a higher rate than its adsorption did, (2) that both the K<sub>a</sub> [TG] and [GL]/K<sub>d</sub> exhibited values equal to zero, (3) that the concentration of the incorporated alcohol [R-OH] was higher than the present TG, and (4) that S<sub>total</sub> values were constant for the studied heterogeneous catalyst. Using the variation in the TG content within the studied system from the start of the reaction ([TG]<sub>0</sub>) up to a certain time interval ([TG]<sub>t</sub>), the equation can be modified to the presented form in Equation (16). The methyl ester conversion (X<sub>(FAME)</sub>) can be derived from the mass balance by Equation (17) and subsequently, Equation (18). The integration of the representative equation of the reaction rate as a function of the methyl ester conversion (X<sub>(FAME)</sub>) resulted in the final equation of the

system (Equation (19)). Therefore, the conversion efficiency as well as the transesterification rate were affected only by the availability or concentrations of TG molecules, suggesting only pseudo- first-order kinetic behavior [1].

$$r_s = d[TG]/dt = K_c[GL] \quad (14)$$

$$K_c = K_a \times K_s \times [R - OH] \times [S_{total}] \quad (15)$$

$$- \ln([TG]_t/[TG]_0) = K_c \times t \quad (16)$$

$$X_{(R-COOCH_3)} = 1 - ([TG]_t/[TG]_0) \quad (17)$$

$$[TG]_t = [TG]_0 \times (1 - X_{(FAME)}) \quad (18)$$

$$- \ln(X_{(R-COOCH_3)}) = K_c \times t \quad (19)$$

### 3.7. The Activation Energy (Ea) and Thermodynamic Functions

The Arrhenius equation (Equation (20)) was used to estimate the activation energies (Ea) of the preformed transesterification reactions in the presence of both Na.SD and K.SD as heterogeneous basic catalysts. The values of Ea were obtained as mathematical parameters for the performance of the linear regression fitting processes of  $\ln(K_c)$  versus the reciprocal values of the experimental activation temperature ( $1/T$ ), where the slope indicates the Ea values and the intercept reflects the pre-exponential value ( $\ln(A)$ ).

$$K_c = A \exp(-Ea/RT) \quad (20)$$

### 3.8. The Thermodynamic Functions

The thermodynamic functions of the transesterification systems of Na.SD and K.SD that occurred were determined based on the Eyring–Polanyi equation (Equation (21)). The included symbols, R, K, h, and  $K_b$ , identify the universal gas constant, rate constant, Planck's constant ( $6.626176 \times 10^{-34}$  Js), and Boltzmann constant ( $1.3806 \times 10^{-23}$  K<sup>-1</sup>). The enthalpy ( $\Delta H^*$ ) and entropy ( $\Delta S^*$ ) values were obtained as parameters of the preformed linear regression plotting of  $\ln(K/T)$  vs. ( $1/T$ ) the slope ( $-H^*/\Delta RT$ ) and intercept. However, the Gibbs free energy ( $\Delta G^*$ ) was calculated using Equation (22).

$$\ln(K/T) = -(\Delta H^*/RT) + \ln(K_b/h) + (\Delta S^*/R) \quad (21)$$

$$\Delta G^* = \Delta H^* - T\Delta S^* \quad (22)$$

## 4. Conclusions

Two sodalite forms, the sodium-rich form (Na.SD) and potassium-rich form (K.SD), were prepared successfully by the low-temperature alkali fusion of kaolinite as potential basic catalysts in the fabrication of biodiesel by transesterification reactions. The Na.SD form confirms the considerable enhancement of catalytic activity and of the essential physicochemical parameters (total basicity: 6.3 mmol OH/g and surface area: 232.4 m<sup>2</sup>/g) compared to K.SD (total basicity: 5.4 mmol OH/g and surface area: 217.6 m<sup>2</sup>/g). The best yield obtained by using Na.SD, this being 97.3%, was maintained at 70 °C, with a 13:1 methanol: oil molar ratio and at a dose of 2.5 wt.% for 90 min, while the best yield that was obtained by K.SD was 95.7%, which was maintained at 70 °C with a 13:1 methanol: oil molar ratio and a dose of 2.5 wt.% for 75 min. Furthermore, the two catalysts showed enhanced recyclability during the four runs; the fifth run of Na.SD showed a slight decrease in the FAME yield to 89%, yet the fifth run of K.SD showed a remarkable decrease to 83%. The kinetic properties (pseudo-first order kinetics) reflected the operation of the transesterification processes according to the progressive steps of adsorption, surface reaction, and desorption. The activation energies of the two transesterification systems as well as the thermodynamic functions (Gibb's free energy, enthalpy, and entropy) signify

the endothermic and spontaneous catalytic reactions that occur when using Na<sub>2</sub>SD and K<sub>2</sub>SD in addition to their significant performances under the low-temperature conditions.

**Supplementary Materials:** The following supporting information can be downloaded at: <https://www.mdpi.com/article/10.3390/catal13030462/s1>, Table S1. The determined fatty acid methyl esters in the obtained biodiesel sample over N<sub>2</sub>SD. Table S2. the Fatty acid content and physical properties of the inspected spent oil

**Author Contributions:** Conceptualization, M.R.A., S.B., J.S.A. and M.A.S.; methodology, M.A.S., J.L. and C.W.; Software, M.A.S., A.A.A. and J.L.; validation, M.R.A., S.B., J.S.A., A.A.A. and C.W.; formal analysis, M.A.S., A.A.A., J.L. and C.W.; investigation, M.R.A., S.B., J.S.A. and A.A.A.; resources, A.A.A., M.A.S., J.L. and C.W.; data curation, M.R.A., M.A.S., J.L. and C.W.; writing—original draft preparation, M.R.A., M.A.S., C.W., A.A.A., S.B., J.S.A., J.L. and C.W.; writing—review and editing, M.R.A., M.A.S., C.W., A.A.A., S.B., J.L. and C.W.; visualization, M.R.A., M.A.S. and S.B.; supervision, M.R.A., S.B., A.A.A. and C.W.; project administration, M.R.A., J.S.A. and A.A.A.; funding acquisition, J.S.A. All authors have read and agreed to the published version of the manuscript.

**Funding:** This research was funded by [King Saud University, Riyadh, Saudi Arabia] grant number [RSP2023R149], [Guangdong Basic and Applied Basic Research Foundation] grant number [2021A1515010060], and [Guangdong Province Scientific Research Platform] grant number [2022ZDZX4046].

**Data Availability Statement:** Data are available upon reasonable, by the Corresponding Authors.

**Acknowledgments:** The authors acknowledge the Researchers Supporting Project (RSP2023R149), King Saud University, Riyadh, Saudi Arabia. The financial support provided by Guangdong Basic and Applied Basic Research Foundation under Grant 2021A1515010060, and in part by Guangdong Province Scientific Research Platform Project under Grant 2022ZDZX4046, is highly appreciated.

**Conflicts of Interest:** The authors declare no conflict of interest.

## References

1. Sayed, M.A.; Ahmed, S.A.; Othman, S.I.; Allam, A.A.; Al Zoubi, W.; Ajarem, J.S.; Abukhadra, M.R.; Bellucci, S. Kinetic, Thermodynamic, and Mechanistic Studies on the Effect of the Preparation Method on the Catalytic Activity of Synthetic Zeolite-A during the Transesterification of Waste Cooking Oil. *Catalysts* **2023**, *13*, 30. [[CrossRef](#)]
2. Rezania, S.; Oryani, B.; Park, J.; Hashemi, B.; Yadav, K.K.; Kwon, E.E.; Hur, J.; Cho, J. Review on transesterification of non-edible sources for biodiesel production with a focus on economic aspects, fuel properties and by-product applications. *Energy Convers. Manag.* **2019**, *201*, 112155. [[CrossRef](#)]
3. Orege, J.I.; Oderinde, O.; Kifle, G.A.; Ibikunle, A.A.; Raheem, S.A.; Ejeromedoghene, O.; Okeke, E.S.; Olukowi, O.M.; Orege, O.B.; Fagbohun, E.O.; et al. Recent advances in heterogeneous catalysis for green biodiesel production by transesterification. *Energy Convers. Manag.* **2022**, *258*, 115406. [[CrossRef](#)]
4. Ali, R.M.; Elkatory, M.R.; Hamad, H.A. Highly active and stable magnetically recyclable CuFe<sub>2</sub>O<sub>4</sub> as a heterogenous catalyst for efficient conversion of waste frying oil to biodiesel. *Fuel* **2020**, *268*, 117297. [[CrossRef](#)]
5. Papargyriou, D.; Broumidis, E.; de Vere-Tucker, M.; Gavrielides, S.; Hilditch, P.; Irvine, J.; Bonaccorso, A.D. Investigation of solid base catalysts for biodiesel production from fish oil. *Renew. Energy* **2019**, *139*, 661–669. [[CrossRef](#)]
6. Kiehadroudzehad, M.; Merabet, A.; Hosseinzadeh-Bandbafha, H. A life cycle assessment perspective on biodiesel production from fish wastes for green microgrids in a circular bioeconomy. *Bioresour. Technol. Rep.* **2023**, *21*, 101303. [[CrossRef](#)]
7. Karmakar, G.; Ghosh, P.; Sharma, B.K. Chemically modifying vegetable oils to prepare green lubricants. *Lubricants* **2017**, *5*, 44. [[CrossRef](#)]
8. Danov, S.M.; Kazantsev, O.A.; Esipovich, A.L.; Belousov, A.S.; Rogozhin, A.E.; Kanakov, E.A. Recent advances in the field of selective epoxidation of vegetable oils and their derivatives: A review and perspective. *Catal. Sci. Technol.* **2017**, *7*, 3659–3675. [[CrossRef](#)]
9. Pleissner, D.; Lau, K.Y.; Zhang, C.; Lin, C.S.K. Plasticizer and surfactant formation from food-waste- and algal biomass-derived lipids. *ChemSusChem* **2015**, *8*, 1686–1691. [[CrossRef](#)]
10. Karis, D.; Cain, R.; Young, K.; Shand, A.; Holm, T.; Springer, E. Non-fuel uses for fatty acid methyl esters. *Biofuels Bioprod. Biorefining* **2022**, *16*, 1893–1908. [[CrossRef](#)]
11. Belousov, A.S.; Esipovich, A.L.; Kanakov, E.A.; Otopkova, K.V. Recent advances in sustainable production and catalytic transformations of fatty acid methyl esters. *Energy Fuels* **2021**, *5*, 4512–4545. [[CrossRef](#)]
12. Sayed, M.R.; Abukhadra, M.R.; Ahmed, S.A.; Shaban, M.; Javed, U.; Betiha, M.A.; Shim, J.-J.; Rabie, A.M. Synthesis of advanced MgAl-LDH based geopolymer as a potential catalyst in the conversion of waste sunflower oil into biodiesel: Response surface studies. *Fuel* **2020**, *282*, 118865. [[CrossRef](#)]

13. Basyouny, M.G.; Abukhadra, M.R.; Alkhaledi, K.; El-Sherbeeney, A.M.; El-Meligy, M.A.; Soliman, A.T.A.; Luqman, M. Insight into the catalytic transformation of the waste products of some edible oils (corn oil and palm oil) into biodiesel using MgO/clinoptilolite green nanocomposite. *Mol. Catal.* **2021**, *500*, 111340. [[CrossRef](#)]
14. Pirouzmand, M.; Anakhatoon, M.M.; Ghasemi, Z. One-step biodiesel production from waste cooking oils over metal incorporated MCM-41; positive effect of template. *Fuel* **2018**, *216*, 296–300. [[CrossRef](#)]
15. Murta, A.L.S.; De Freitas, M.A.V.; Ferreira, C.G.; Peixoto, M.M.D.C.L. The use of palm oil biodiesel blends in locomotives: An economic, social and environmental analysis. *Renew. Energy* **2021**, *164*, 521–530. [[CrossRef](#)]
16. Malhotra, R.; Ali, A. 5-Na/ZnO doped mesoporous silica as reusable solid catalyst for biodiesel production via transesterification of virgin cottonseed oil. *Renew. Energy* **2019**, *133*, 606–619. [[CrossRef](#)]
17. Sai, B.A.V.S.L.; Subramaniapillai, N.; Mohamed, M.S.B.K.; Narayanan, A. Optimization of continuous biodiesel production from rubber seed oil (RSO) using calcined eggshells as heterogeneous catalyst. *J. Environ. Chem. Eng.* **2020**, *8*, 103603. [[CrossRef](#)]
18. Hoseini, S.; Najafi, G.; Sadeghi, A. Chemical characterization of oil and biodiesel from Common Purslane (*Portulaca*) seed as novel weed plant feedstock. *Ind. Crops Prod.* **2019**, *140*, 111582. [[CrossRef](#)]
19. Ibrahim, M.L.; Nik Abdul Khalil, N.N.A.; Islam, A.; Rashid, U.; Ibrahim, S.F.; Sinar Mashuri, S.I.; Taufiq-Yap, Y.H. Preparation of Na<sub>2</sub>O supported CNTs nanocatalyst for efficient biodiesel production from waste-oil. *Energy Convers. Manag.* **2020**, *205*, 112445. [[CrossRef](#)]
20. Bin Jumah, M.N.; Ibrahim, S.M.; Al-Huqail, A.A.; Bin-Murthi, N.S.; Allam, A.A.; Abu-Taweel, G.M.; Altoom, N.; Al-Anazi, K.M.; Abukhadra, M.R. Enhancing the catalytic performance of NiO during the transesterification of waste cooking oil using a diatomite carrier and an integrated NiO/Metal: Response surface studies. *ACS Omega* **2021**, *6*, 12318–12330. [[CrossRef](#)]
21. Banković-Ilić, I.B.; Stamenković, O.S.; Veljković, V.B. Biodiesel production from non-edible plant oils. *Renew. Sustain. Energy Rev.* **2012**, *16*, 3621–3647. [[CrossRef](#)]
22. Takase, M.; Zhang, M.; Feng, W.; Chen, Y.; Zhao, T.; Cobbina, S.J.; Yang, L.; Wu, X. Application of zirconia modified with KOH as heterogeneous solid base catalyst to new non-edible oil for biodiesel. *Energy Convers. Manag.* **2014**, *80*, 117–125. [[CrossRef](#)]
23. Sharma, Y.C.; Singh, B.; Korstad, J. Latest developments on application of heterogenous basic catalysts for an efficient and eco friendly synthesis of biodiesel: A review. *Fuel* **2011**, *90*, 1309–1324. [[CrossRef](#)]
24. Mukhtar, A.; Saqib, S.; Lin, H.; Shah, M.U.H.; Ullah, S.; Younas, M.; Rezakazemi, M.; Ibrahim, M.; Mahmood, A.; Asif, S.; et al. Current status and challenges in the heterogeneous catalysis for biodiesel production. *Renew. Sustain. Energy Rev.* **2022**, *157*, 112012. [[CrossRef](#)]
25. Lee, J.-S.; Saka, S. Biodiesel production by heterogeneous catalysts and supercritical technologies. *Bioresour. Technol.* **2010**, *101*, 7191–7200. [[CrossRef](#)]
26. Brahma, S.; Basumatary, B.; Basumatary, S.F.; Das, B.; Brahma, S.; Rokhum, S.L.; Basumatary, S. Biodiesel production from quinary oil mixture using highly efficient *Musa chinensis* based heterogeneous catalyst. *Fuel* **2023**, *336*, 127150. [[CrossRef](#)]
27. Fattahi, N.; Triantafyllidis, K.; Luque, R.; Ramazani, A. Zeolite-based catalysts: A valuable approach toward ester bond formation. *Catalysts*. **2019**, *9*, 758. [[CrossRef](#)]
28. Otieno, S.O.; Kowenje, C.O.; Okoyo, A.; Onyango, D.M.; Amisi, K.O.; Nzioka, K.M. Optimizing production of biodiesel catalysed by chemically tuned natural zeolites. *Mater. Today Proc.* **2018**, *5*, 10561–10569. [[CrossRef](#)]
29. Li, Z.; Ding, S.; Chen, C.; Qu, S.; Du, L.; Lu, J.; Ding, J. Recyclable Li/NaY zeolite as a heterogeneous alkaline catalyst for biodiesel production: Process optimization and kinetics study. *Energy Convers. Manag.* **2019**, *192*, 335–345. [[CrossRef](#)]
30. Nasief, F.; Shaban, M.; Alamry, K.A.; Abu Khadra, M.R.; Khan, A.A.P.; Asiri, A.M.; El-Salam, H.A. Hydrothermal synthesis and mechanically activated zeolite material for utilizing the removal of Ca/Mg from aqueous and raw groundwater. *J. Environ. Chem. Eng.* **2021**, *9*, 105834. [[CrossRef](#)]
31. Simanjuntak, W.; Pandiangan, K.D.; Sembiring, Z.; Simanjuntak, A.; Hadi, S. The effect of crystallization time on structure, microstructure, and catalytic activity of zeolite-A synthesized from rice husk silica and food-grade aluminum foil. *Biomass Bioenergy* **2021**, *148*, 106050. [[CrossRef](#)]
32. Abukhadra, M.R.; Othman, S.I.; Allam, A.A.; Elfayoumi, H. Insight into the catalytic properties zeolitized kaolinite/diatomite geopolymer as an environmental catalyst for the sustainable conversion of spent cooking oil into biodiesel; optimization and kinetics. *Sustain. Chem. Pharm.* **2021**, *22*, 100473. [[CrossRef](#)]
33. Rios, C.; Williams, C.; Fullen, M. Nucleation and growth history of zeolite LTA synthesized from kaolinite by two different methods. *Appl. Clay Sci.* **2009**, *42*, 446–454. [[CrossRef](#)]
34. Mokrzycki, J.; Fedyna, M.; Marzec, M.; Panek, R.; Szerement, J.; Marcińska-Mazur, L.; Jarosz, R.; Bajda, T.; Franus, W.; Mierzwa-Hersztek, M. The influence of zeolite X ion-exchangeable forms and impregnation with copper nitrate on the adsorption of phosphate ions from aqueous solutions. *J. Water Process Eng.* **2022**, *50*, 103299. [[CrossRef](#)]
35. Alismael, Z.T.; Al-Jadir, T.M.; Albayati, T.M.; Abbas, A.S.; Doyle, A.M. Modification of FAU zeolite as an active heterogeneous catalyst for biodiesel production and theoretical considerations for kinetic modeling. *Adv. Powder Technol.* **2022**, *33*, 103646. [[CrossRef](#)]
36. Salam, M.A.; Abukhadra, M.R.; Mostafa, M. Effective decontamination of As(V), Hg(II), and U(VI) toxic ions from water using novel muscovite/zeolite aluminosilicate composite: Adsorption behavior and mechanism. *Environ. Sci. Pollut. Res.* **2020**, *27*, 13247–13260. [[CrossRef](#)]

37. Ayele, L.; Pérez-Pariente, J.; Chebude, Y.; Díaz, I. Conventional versus alkali fusion synthesis of zeolite A from low grade kaolin. *Appl. Clay Sci.* **2016**, *132–133*, 485–490. [[CrossRef](#)]
38. Altoom, N.; Adlii, A.; Othman, S.I.; Allam, A.A.; Alqhtani, H.A.; Al-Otaibi, F.S.; Abukhadra, M.R. Synthesis and characterization of  $\beta$ -cyclodextrin functionalized zeolite-A as biocompatible carrier for Levofloxacin drug; loading, release, cytotoxicity, and anti-inflammatory studies. *J. Solid State Chem.* **2022**, *312*, 123280. [[CrossRef](#)]
39. Shaban, M.; Sayed, M.I.; Shahien, M.G.; Abukhadra, M.R.; Ahmed, Z.M. Adsorption behavior of inorganic- and organic-modified kaolinite for Congo red dye from water, kinetic modeling, and equilibrium studies. *J. Sol-Gel Sci. Technol.* **2018**, *87*, 427–441. [[CrossRef](#)]
40. Sakızci, M.; Özer, M. The characterization and methane adsorption of Ag-, Cu-, Fe-, and H-exchanged chabazite-rich tuff from Turkey. *Environ. Sci. Pollut. Res.* **2019**, *26*, 16616–16627. [[CrossRef](#)]
41. Mostafa, M.; El-Meligy, M.A.; Sharaf, M.; Soliman, A.T.; AbuKhadra, M.R. Insight into chitosan/zeolite-A nanocomposite as an advanced carrier for levofloxacin and its anti-inflammatory properties; loading, release, and anti-inflammatory studies. *Int. J. Biol. Macromol.* **2021**, *179*, 206–216. [[CrossRef](#)]
42. Abukhadra, M.R.; Sayed, M.A.  $K^+$  trapped kaolinite (Kaol/ $K^+$ ) as low cost and eco-friendly basic heterogeneous catalyst in the transesterification of commercial waste cooking oil into biodiesel. *Energy Convers. Manag.* **2018**, *177*, 468–476. [[CrossRef](#)]
43. Arana, J.T.; Torres, J.J.; Acevedo, D.F.; Illanes, C.O.; Ochoa, N.A.; Pagliero, C.L. One-step synthesis of CaO-ZnO efficient catalyst for biodiesel production. *Int. J. Chem. Eng.* **2019**, *2019*, 1806017. [[CrossRef](#)]
44. Roy, T.; Sahani, S.; Sharma, Y.C. Study on kinetics-thermodynamics and environmental parameter of biodiesel production from waste cooking oil and castor oil using potassium modified ceria oxide catalyst. *J. Clean. Prod.* **2020**, *247*, 119166. [[CrossRef](#)]
45. Ayoub, M.; Bhat, A.H.; Ullah, S.; Ahmad, M.; Uemura, Y. Optimization of Biodiesel Production over Alkaline Modified Clay Catalyst. *J. Japan Inst. Energy.* **2017**, *96*, 456–462. [[CrossRef](#)]
46. Seela, C.R.; Alagumalai, A.; Pugazhendhi, A. Evaluating the feasibility of diethyl ether and isobutanol added Jatropha Curcas biodiesel as environmentally friendly fuel blends. *Sustain. Chem. Pharm.* **2020**, *18*, 100340. [[CrossRef](#)]
47. Ibrahim, S.M.; El-Sherbeeney, A.M.; Shim, J.-J.; AlHammadi, A.A.; Abukhadra, M.R.  $-SO_3H$ -functionalization of sub-bituminous coal as a highly active acidic catalyst during the transesterification of spent sunflower oil; characterization, application, and mechanism. *Energy Rep.* **2021**, *7*, 8699–8710. [[CrossRef](#)]
48. Salim, S.M.; Izriq, R.; Almaky, M.M.; Al-Abbassi, A.A. Synthesis and characterization of ZnO nanoparticles for the production of biodiesel by transesterification: Kinetic and thermodynamic studies. *Fuel* **2022**, *321*, 124135. [[CrossRef](#)]
49. Gardy, J.; Rehan, M.; Hassanpour, A.; Lai, X.; Nizami, A.-S. Advances in nano-catalysts based biodiesel production from non-food feedstocks. *J. Environ. Manag.* **2019**, *249*, 109316. [[CrossRef](#)]
50. Rabie, A.M.; Shaban, M.; Abukhadra, M.R.; Hosny, R.; Ahmed, S.A.; Negm, N.A. Diatomite supported by CaO/MgO nanocomposite as heterogeneous catalyst for biodiesel production from waste cooking oil. *J. Mol. Liq.* **2019**, *279*, 224–231. [[CrossRef](#)]
51. Bhatia, S.K.; Gurav, R.; Choi, T.-R.; Kim, H.J.; Yang, S.-Y.; Song, H.-S.; Park, J.Y.; Park, Y.-L.; Han, Y.-H.; Choi, Y.-K.; et al. Conversion of waste cooking oil into biodiesel using heterogenous catalyst derived from cork biochar. *Bioresour. Technol.* **2020**, *302*, 122872. [[CrossRef](#)]
52. Singh, V.; Bux, F.; Sharma, Y.C. A low cost one pot synthesis of biodiesel from waste frying oil (WFO) using a novel material,  $\beta$ -potassium dizirconate ( $\beta$ - $K_2Zr_2O_5$ ). *Appl. Energy* **2016**, *172*, 23–33. [[CrossRef](#)]
53. Abukhadra, M.R.; Soliman, S.R.; Bin Jumah, M.N.; Othman, S.I.; AlHammadi, A.A.; Alruhaimi, R.S.; Albohairy, F.M.; Allam, A.A. Insight into the sulfonation conditions on the activity of sub-bituminous coal as acidic catalyst during the transesterification of spent corn oil; effect of sonication waves. *Sustain. Chem. Pharm.* **2022**, *27*, 100691. [[CrossRef](#)]
54. Bellucci, S.; Eid, M.H.; Fekete, I.; Péter, S.; Kovács, A.; Othman, S.I.; Ajarem, J.S.; Allam, A.A.; Abukhadra, M.R. Synthesis of  $K^+$  and  $Na^+$  Synthetic Sodalite Phases by Low-Temperature Alkali Fusion of Kaolinite for Effective Remediation of Phosphate Ions: The Impact of the Alkali Ions and Realistic Studies. *Inorganics* **2023**, *11*, 14. [[CrossRef](#)]
55. Kamel, D.A.; Farag, H.A.; Amin, N.K.; Zatout, A.A.; Ali, R.M. Smart utilization of jatropha (*Jatropha curcas* Linnaeus) seeds for biodiesel production: Optimization and mechanism. *Ind. Crops Prod.* **2018**, *111*, 407–413. [[CrossRef](#)]
56. Kouzu, M.; Kasuno, T.; Tajika, M.; Sugimoto, Y.; Yamanaka, S.; Hidaka, J. Calcium oxide as a solid base catalyst for transesterification of soybean oil and its application to biodiesel production. *Fuel* **2008**, *87*, 2798–2806. [[CrossRef](#)]
57. Yang, X.-X.; Wang, Y.-T.; Yang, Y.-T.; Feng, E.-Z.; Luo, J.; Zhang, F.; Yang, W.-J.; Bao, G.-R. Catalytic transesterification to biodiesel at room temperature over several solid bases. *Energy Convers. Manag.* **2018**, *164*, 112–121. [[CrossRef](#)]
58. Chen, G.; Shan, R.; Li, S.; Shi, J. A biomimetic silicification approach to synthesize CaO-SiO<sub>2</sub> catalyst for the transesterification of palm oil into biodiesel. *Fuel* **2015**, *153*, 48–55. [[CrossRef](#)]
59. Aghel, B.; Mohadesi, M.; Ansari, A.; Maleki, M. Pilot-scale production of biodiesel from waste cooking oil using kettle limescale as a heterogeneous catalyst. *Renew. Energy* **2019**, *142*, 207–214. [[CrossRef](#)]
60. Babajide, O.; Musyoka, N.; Petrik, L.; Ameer, F. Novel zeolite Na-X synthesized from fly ash as a heterogeneous catalyst in biodiesel production. *Catal. Today* **2012**, *190*, 54–60. [[CrossRef](#)]
61. Maneerung, T.; Kawi, S.; Wang, C.-H. Biomass gasification bottom ash as a source of CaO catalyst for biodiesel production via transesterification of palm oil. *Energy Convers. Manag.* **2015**, *92*, 234–243. [[CrossRef](#)]
62. Amani, H.; Asif, M.; Hameed, B. Transesterification of waste cooking palm oil and palm oil to fatty acid methyl ester using cesium-modified silica catalyst. *J. Taiwan Inst. Chem. Eng.* **2016**, *58*, 226–234. [[CrossRef](#)]

63. Abukhadra, M.R.; Dardir, F.M.; Shaban, M.; Ahmed, E.A.; Soliman, M.F. Spongy Ni/Fe carbonate-fluorapatite catalyst for efficient conversion of cooking oil waste into biodiesel. *Environ. Chem. Lett.* **2018**, *16*, 665–670. [[CrossRef](#)]
64. Thushari, I.; Babel, S.; Samart, C. Biodiesel production in an autoclave reactor using waste palm oil and coconut coir husk derived catalyst. *Renew. Energy* **2019**, *134*, 125–134. [[CrossRef](#)]
65. Lima, A.C.; Hachemane, K.; Ribeiro, A.E.; Queiroz, A.; Gomes, M.C.S.; Brito, P. Evaluation and kinetic study of alkaline ionic liquid for biodiesel production through transesterification of sunflower oil. *Fuel* **2022**, *324*, 124586. [[CrossRef](#)]
66. Jain, S.; Sharma, M.; Rajvanshi, S. Acid base catalyzed transesterification kinetics of waste cooking oil. *Fuel Process. Technol.* **2011**, *92*, 32–38. [[CrossRef](#)]
67. Hassan, W.A.; Ahmed, E.A.; Moneim, M.A.; Shaban, M.S.; El-Sherbeeney, A.M.; Siddiqui, N.; Shim, J.-J.; Abukhadra, M.R. Sulfonation of Natural Carbonaceous Bentonite as a Low-Cost Acidic Catalyst for Effective Transesterification of Used Sunflower Oil into Diesel; Statistical Modeling and Kinetic Properties. *ACS Omega* **2021**, *6*, 31260–31271. [[CrossRef](#)]

**Disclaimer/Publisher’s Note:** The statements, opinions and data contained in all publications are solely those of the individual author(s) and contributor(s) and not of MDPI and/or the editor(s). MDPI and/or the editor(s) disclaim responsibility for any injury to people or property resulting from any ideas, methods, instructions or products referred to in the content.